A Linear Model Approach for Ultrasonic Inverse Problems With Attenuation and Dispersion

Ewen Carcreff, Sébastien Bourguignon, Jérôme Idier, *Member, IEEE*, and Laurent Simon, *Member, IEEE*

***Abstract*—Ultrasonic inverse problems such as spike train deconvolution, synthetic aperture focusing, or tomography attempt to reconstruct spatial properties of an object (discontinuities, delaminations, flaws, etc.) from noisy and incomplete measurements. They require an accurate description of the data acquisition process. Dealing with frequency-dependent attenuation and dispersion is therefore crucial because both phenomena modify the wave shape as the travel distance increases. In an inversion context, this paper proposes to exploit a linear model of ultrasonic data taking into account attenuation and dispersion. The propagation distance is discretized to build a finite set of radiation impulse responses. Attenuation is modeled with a frequency power law and then dispersion is computed to yield physically consistent responses. Using experimental data acquired from attenuative materials, this model outperforms the standard attenuation-free model and other models of the literature. Because of model linearity, robust estimation methods can be implemented. When matched filtering is employed for single echo detection, the model that we propose yields precise estimation of the attenuation coefficient and of the sound velocity. A thickness estimation problem is also addressed through spike deconvolution, for which the proposed model also achieves accurate results.**

I. Introduction

Ultrasonic waves are widely used for nondestructive testing (NDT) of materials [1], [2], tissue characterization [3] and biomedical imaging [4], [5]. Many applications in these fields can be formulated as inverse problems such as spike train deconvolution [6]–[8], biomedical image restoration [4], [9], time-of-flight tomography [10]–[12] and synthetic aperture focusing techniques (SAFT) [13]–[15]. Such problems rely on both an accurate direct model describing the acquisition process and appropriate prior information constraining the solution [8].

Attenuation and dispersion can arise in the aforementioned applications. Attenuation is due to two basic causes; namely, scattering and absorption. Scattering results from the fact that the material is not strictly homogeneous, implying multiple direction propagation. Absorption is caused by the excitation of the particles that converts sound energy into heat. Consequently, attenuation increases with frequency. Most models in the literature consider a frequency power law [3], [16]. This frequency-dependent loss has a low-pass filtering effect on the transmitted waves and grows as propagation distance increases. It generates a shape broadening of the echoes that degrades the resolution [17]. Dispersion—a by-product of attenuation—means that the phase velocity depends on frequency, producing a frequency-dependent phase variation of the echoes [5], [17], [18].

Attenuation and dispersion are often overlooked in ultrasonic direct models for inversion purposes. Most formulations consider a linear model that is invariant with respect to the propagation distance. However, if the ultrasonic propagation characteristics are not considered, the performance of the algorithms can be degraded because the model accuracy is too weak. Several approaches have been developed to include attenuation in acoustical inverse problems, mostly in geophysics [19]–[21]. Indeed, similar effects impact the propagation of seismic waves that is modeled as the Q-filter [19], [22]. In the field of ultrasonic NDT, some methods overcome the issue of wave distortion by proposing a greater flexibility in the direct model. On the one hand, parametric methods associate a specific shape to each echo, which is usually modeled as a modulated Gaussian pulse. The parameters of each echo are then estimated by nonlinear least-squares fitting [23] or by greedy procedures such as matching pursuit [24]–[26]. On the other hand, nonparametric approaches employ a blind strategy in which weaker constraints are imposed on the echo shape—as, for example, slow variations between neighboring intervals of the propagation distance [27]. Even if such models allow for some shape variation of the echoes with respect to the propagation distance, they do not introduce any physical knowledge about the propagation properties.

The goal of the present paper is to contribute to the solving of ultrasonic inverse problems by including attenuation and dispersion in the direct model. In particular, we propose to account for physical attenuation profiles defined in the frequency domain like power law attenuation models. Our objective is threefold. First, we improve the ultrasound model accuracy compared with the standard attenuation-free model. Second, in contrast with the aforementioned methods [23]–[27], we yield a more constrained description of the data. Consequently, better performance of the inversion procedure is expected. In particular, a more accurate model aims at improving echo detection for

Manuscript received January 18, 2014; accepted April 18, 2014. This work was partially supported by the French Région Pays de la Loire as part of the scientific program Non-Destructive Testing and Evaluation–Pays de la Loire (ECND-PdL).

E. Carcreff, S. Bourguignon, and J. Idier are with the Institut de Recherche en Communications et Cybernétique de Nantes (IRCCyN), Nantes, France (e-mail: ewen.carcreff@irccyn.ec-nantes.fr).

E. Carcreff and L. Simon are with the Laboratoire d'Acoustique de l'Université du Maine (LAUM), Le Mans, France.

DOI http://dx.doi.org/10.1109/TUFFC.2014.3018

long propagation distances where the signal-to-noise ratio is low. Last, our framework yields a linear direct model which enables the use of many acknowledged inversion methods [8]. Related works [7], [28] proposed similar approaches but with an empirical description of attenuation within a time-domain signal model. The model that we propose is derived from the physics of wave propagation and is described in the frequency domain [3], [16].

In this paper, the signal model is formulated as a set of transfer functions in the Fourier domain [29]. The propagation in the medium is modeled by a so-called radiation transfer function [30] depending on the wavenumber $k(f) = \beta(f) - j\alpha(f)$. The term $\beta(f)$ is related to the phase velocity and $\alpha(f)$ is the attenuation. To ensure the consistency of the corresponding radiation impulse response, $\alpha(f)$ and $\beta(f)$ are analytically linked by conditions derived from the Kramers–Kronig relations [31]. Several models have been developed, both for continuous-time and discrete-time signals, and validated for materials having linear and nonlinear attenuation [31]–[34]. In this paper, we will use the formulation proposed by Kuc [35], [36]. Because attenuation depends on propagation distance, we build a set of radiation impulse responses by an appropriate discretization of the space domain. We then obtain a discrete linear model of data $\mathbf{y} = \mathbf{H}_\mathrm{e}\mathbf{H}_\mathrm{a}\mathbf{x}$. The matrix $\mathbf{H}_\mathrm{e}$ represents the instrumental response, which is invariant with respect to the propagation distance. The matrix $\mathbf{H}_\mathrm{a}$ stands for the set of radiation impulse responses. The vector $\mathbf{x}$ represents the unknown spatial distribution of targets. Note that standard direct models consider an invariant model with respect to the propagation distance; that is, $\mathbf{y} = \mathbf{H}_\mathrm{e}\mathbf{x}$.

A major advantage of the obtained model is in its generality for a large variety of ultrasonic inverse problems. The purpose of inversion is then to estimate the object $\mathbf{x}$ based on the knowledge of $\mathbf{y}$, $\mathbf{H}_\mathrm{e}$, and $\mathbf{H}_\mathrm{a}$, and on some prior information on $\mathbf{x}$. In NDT for example, $\mathbf{x}$ is expected to have a few nonzero elements, corresponding to the positions of impedance discontinuities, including flaws [6]. The description and the validation of sophisticated inversion algorithms are out of the scope of this paper. Consequently, experiments are dedicated to rather simple estimation problems in homogeneous plates. We use two basic inverse methods, namely, a matched filtering procedure and an ℓ_1-norm-based spike train deconvolution method [6] applied to non-overlapping echoes.

The paper is organized as follows. Section II describes the model of ultrasonic signals, defined in the frequency domain. The relation proposed by Kuc [35] between the phase and the magnitude of the radiation transfer function is detailed. The model is validated on experimental data acquired in a polymethyl methacrylate (PMMA) plate. Then, in Section III, a linear direct model is built, based on the discretization of the unknown spatial source distribution. Such a frequency-based approach is compared with Olofsson's time-domain model [7]. In Section IV, experimental results are shown through the nondestructive evaluation of a polycarbonate plate to estimate the attenuation coefficient and the velocity. Section V considers a typical plate thickness estimation problem in which a spike train deconvolution method is considered using our model. The paper ends with a discussion in Section VI.

II. Propagation Model of Ultrasonic Signals

A. Model for a Single Target

Here, the ultrasonic measurement is made in a homogeneous and isotropic medium containing a single point-like target placed at spatial location $\mathbf{r}_\mathrm{T}$. The configuration can either use two transducers, a transmitter and a receiver (T/R), or a single transducer in pulse–echo (P/E) mode—see Fig. 1 for the description of both configurations. The received signal can be defined in the Fourier domain by a set of transfer functions [29], [37]:

$$Y(f, \mathbf{r}_\mathrm{T}) = U(f)H_\mathrm{ea}(f)H_\mathrm{r}(f, \mathbf{r}_\mathrm{T})H_\mathrm{ae}(f), \tag{1}$$

as illustrated in Fig. 2. $U(f)$ is the electrical excitation pulse sent to the emitting transducer. The functions $H_\mathrm{ea}(f)$ and $H_\mathrm{ae}(f)$ are the electro-acoustical and acousto-electrical frequency responses of the transducers, respectively. The global instrumental function $H_\mathrm{e}(f) = U(f)H_\mathrm{ea}(f)H_\mathrm{ae}(f)$ can be defined by collecting the functions that do not depend on the propagation in the material. The received spectrum is therefore

$$Y(f, \mathbf{r}_\mathrm{T}) = H_\mathrm{e}(f)H_\mathrm{r}(f, \mathbf{r}_\mathrm{T}). \tag{2}$$

The radiation transfer function $H_\mathrm{r}(f, \mathbf{r}_\mathrm{T})$ represents the transfer function related to the propagation path [29], [30]. As an example, let us consider the one-way path from the emitting transducer with surface S to the target. The radiation transfer function[1] in $\mathbf{r}_\mathrm{T}$ is the sum over elementary contributions of sources over the surface S [30]:

$$H^1_\mathrm{r}(f, \mathbf{r}_\mathrm{T}) = \int_{\mathbf{r}_0 \in S} \frac{e^{-jk(f)\|\mathbf{r}_\mathrm{T} - \mathbf{r}_0\|}}{2\pi\|\mathbf{r}_\mathrm{T} - \mathbf{r}_0\|} \mathrm{d}S. \tag{3}$$

In T/R mode, as represented in Fig. 1, the overall radiation transfer function is the product of two different radiation functions (transmitter to target and target to receiver), whereas in P/E mode, the two transfer functions are equal [38]. Note that one could consider specific target surfaces, leading to different reflector signatures [37]. For example, Lhémery has developed a model with small oriented targets, including the diffraction of the transducers [38]. In the current paper, we consider targets with identical signatures.

The complex-valued frequency-dependent wavenumber $k(f)$ can be written

[1] By convention, for a frequency f, we consider a plane wave $e^{j(2\pi ft - k(f)x)}$ propagating in the positive x direction, where $k(f)$ is the wavenumber.

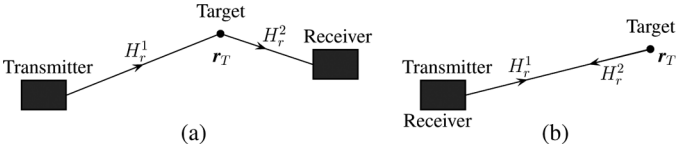

Fig. 1. Two possible configurations for ultrasonic data aquisition: (a) transmit–receive mode and (b) pulse–echo mode.

$$k(f) = \beta(f) - j\alpha(f). \tag{4}$$

The term $\beta(f)$ describes the propagation of the wave such that $\beta(f) = 2\pi f/c(f)$, where $c(f)$ is the phase velocity. The term $\alpha(f)$ represents the attenuation in the material. By neglecting the diffraction of the transducers, we assume that the distance of propagation is roughly constant for all points of the radiating and receiving surfaces [29]. Let z represent the distance of the travel path from the center of the emitter to the center of the receiver through the target. From (3) and (4), one can write the radiation transfer function:

$$\begin{aligned} H_{\mathrm{r}}(f,z) &= b(z)e^{-\alpha(f)z}e^{-j\beta(f)z} \\ &= b(z)e^{-\alpha(f)z}e^{-j2\pi fz/c(f)}. \end{aligned} \tag{5}$$

The frequency-independent term $b(z)$ depends on the propagation distance and on several factors such as the transducer and target surfaces and their relative positions. For each z, the radiation impulse response $h_{\mathrm{r}}(t,z)$ is given by the inverse Fourier transform of $H_{\mathrm{r}}(f,z)$. Similarly, $h_{\mathrm{e}}(t)$ is the impulse response corresponding to $H_{\mathrm{e}}(f)$. From (2), the time-domain signal received by the transducer for a single target is

$$y(t,z) = h_{\mathrm{e}}(t) * h_{\mathrm{r}}(t,z), \tag{6}$$

which is the convolution between the instrumental impulse response $h_{\mathrm{e}}(t)$ and the radiation impulse response $h_{\mathrm{r}}(t,z)$ depending on the propagation distance z.

Most ultrasound propagation models in tissue characterization and NDT consider a frequency power law attenuation model [16]:

$$\alpha(f) = \alpha_0|f|^{\gamma}, \tag{7}$$

where α_0 and γ are real positive parameters characterizing a given material. Generally, the frequency power parameter satisfies $1 \leq \gamma \leq 2$ [16], [34]. For tissues, one typically has $1 \leq \gamma \leq 1.5$ [39]. Many materials have linear attenuation, that is, $\gamma = 1$ [3], [32]. Numerous methods have been proposed to measure the parameter α_0 in such a case [3], [35], [36], [40]. In NDT, $\gamma > 1$ corresponds to nonlinear attenuation and is related to more complex material structures, for instance, polyethylene ($\gamma \approx 1.13$), synthetic rubber ($\gamma \approx 1.38$), or castor oil ($\gamma \approx 1.67$) [34], [40].

Note that the attenuation model (7) is similar to the constant-Q model employed in geophysics for seismic waves [22]. Q is a quality factor and can be defined as $Q = \pi/\alpha_0 c_0$, if c_0 is the constant wave velocity [21]. The parameter Q is also inversely proportional to α_0, meaning that infinite Q corresponds to a lossless medium ($\alpha_0 = 0$). Similarly, it has been shown that propagation in soils is adequately modeled with $\gamma \in [1,2]$ [21].

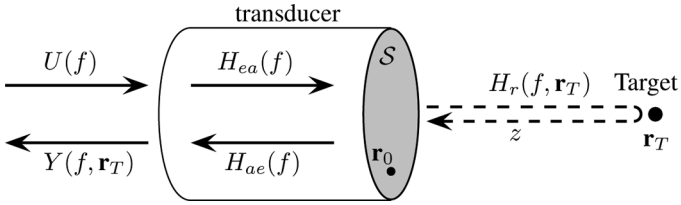

Fig. 2. Pulse–echo measurement for a target located at $\mathbf{r}_{\mathrm{T}}$ using a radiating surface $\mathcal{S}$. The received signal $Y(f,\mathbf{r}_{\mathrm{T}})$ is modeled through a set of transfer functions: $Y(f,\mathbf{r}_{\mathrm{T}}) = U(f)H_{\mathrm{ea}}(f)H_{\mathrm{r}}(f,\mathbf{r}_{\mathrm{T}})H_{\mathrm{ae}}(f)$. z is the overall propagation distance.

From (5) and (7), attenuation has a low-pass effect, causing a downshift of the center frequency of the echoes as the propagation distance increases [16], [17], [41] and limiting the resolution. Such an effect is represented in Fig. 3(a), which shows a typical radiation transfer function $|H_{\mathrm{r}}(f,z)|$ as a function of both frequency f and propagation distance z. This implies the use of relatively low-frequency transducers and a strong amplitude loss for long distances. In the time domain, this effect causes a broadening of the echoes that lessens the resolution as the distance increases.

B. Causality of the Radiation Impulse Response

For physical reality purpose, constraints are applied on the radiation impulse response $h_{\mathrm{r}}(t,z)$. First, the response is real-valued and therefore implies the Hermitian symmetry property $H_{\mathrm{r}}(-f,z)^* = H_{\mathrm{r}}(f,z)$, where the asterisk stands for complex conjugation. As a consequence, according to (4) and (5), the wavenumber has the anti-Hermitian symmetry property, leading to $\alpha(f)$ even and $\beta(f)$ odd. Second, in acoustics, the phase velocity $c(f)$ increases as a function of frequency, which is called the anomalous dispersion [34]. Therefore, there exists a maximum velocity for $f = \infty$ [42], say, c_0. For a given distance z, this maximum velocity is directly linked to a minimum time of flight $t_0 = z/c_0$ such that $h_{\mathrm{r}}(t,z) = 0$ for $t < t_0$. In other words, an ultrasonic wave emitted at $t = 0$ should not appear before t_0 for a target located at distance z. Note that c_0 is larger than the group velocity, which is the velocity of the envelope of the waveform. Such causality principle implies specific relations between the phase and the magnitude in (5) [34], [43].

Kak and Dines [3] proposed a linear phase model, under a linear attenuation assumption $\alpha(f) = \alpha_0|f|$, by considering a constant phase velocity $c(f) = c_0$:

$$H_{\mathrm{r}}(f,z) = b(z)e^{-\alpha(f)z}e^{-j2\pi fz/c_0}. \tag{8}$$

In this case, c_0 also corresponds to the group velocity. The inverse Fourier transform of $e^{-j2\pi fz/c_0}$ is a delta function

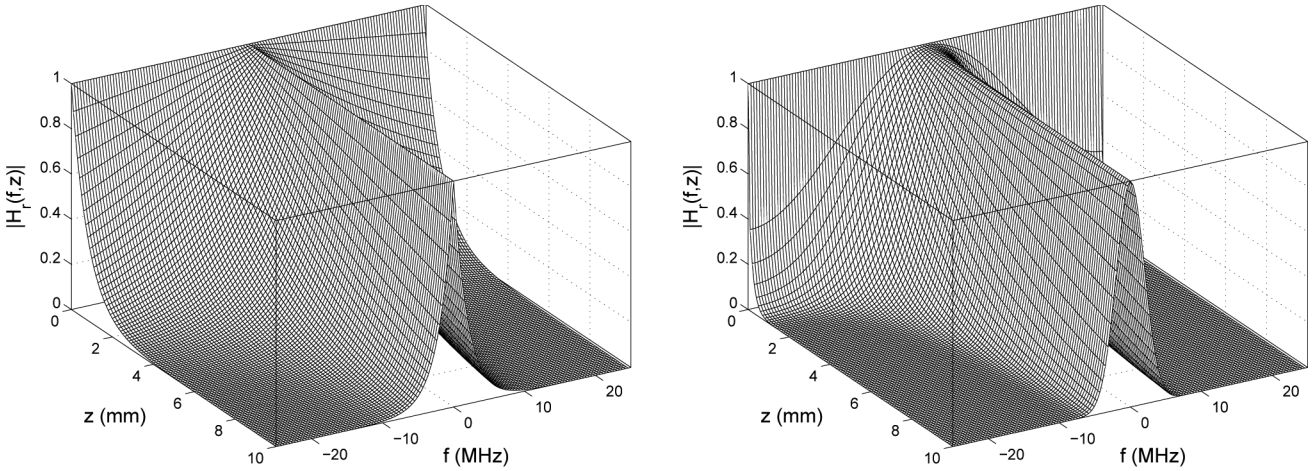

Fig. 3. Examples of attenuation as a function of frequency f and of propagation distance z. The larger the distance, the more important is the low-pass filtering effect of attenuation. (a) Linear attenuation model: $|H_{\rm r}(f,z)| = e^{-\alpha_0|f|z}$, with $\alpha_0 = 50$ Np/MHz/m. (b) Olofsson's model [7] with $\alpha = 0.2$ (see Section III-C).

$\delta(t - z/c_0)$ corresponding to a pure delay of $t_0 = z/c_0$. However, under this linear phase assumption, the impulse response $h_{\rm r}(t,z)$ is symmetric with respect to t_0 and hence is not causal [3].

Indeed, the Paley–Wiener condition states that $h_{\rm r}(t,z)$ is causal if and only if [44]

$$\int_{-\infty}^{+\infty} \frac{|\ln|H_{\rm r}(f,z)||}{1+f^2}\,{\rm d}f < \infty. \tag{9}$$

In such a case, the corresponding phase term is derived from the Kramers–Kronig relations [31], [44]. For the power law attenuation model (7), equation (9) is verified only for $\gamma < 1$ [40], [42], [43]; that is, $h_{\rm r}(t,z)$ is not causal for $\gamma \geq 1$.

Gurumurthy and Arthur [32] considered a minimum-phase model [44], [45] accounting for dispersion in the case $\gamma = 1$. They considered that attenuation grows only sub-linearly at high frequencies to compute the dispersion from the Kramers–Kronig relations [32]. Nevertheless, this model is not strictly causal because the Paley–Wiener condition is not respected. A dispersion term $\varepsilon(f)$ is added to the linear phase term in (8), which yields

$$H_{\rm r}(f,z) = b(z)e^{-\alpha(f)z}e^{-j2\pi fz/c_0}e^{-j\varepsilon(f)z}. \tag{10}$$

$H_{\rm r}(f,z)$ can then be separated into the linear-phase function $b(z)e^{-j2\pi fz/c_0}$ and the attenuation function:

$$H_{\rm a}(f,z) = e^{-\alpha(f)z}e^{-j\varepsilon(f)z}, \tag{11}$$

that is, in the time domain:

$$\begin{aligned} h_r(t,z) &= b(z)h_{\rm a}(t,z) * \delta(t - z/c_0) \\ &= b(z)h_{\rm a}(t - z/c_0, z), \end{aligned} \tag{12}$$

with $h_{\rm a}(t,z)$ the attenuation impulse response corresponding to $H_{\rm a}(f,z)$.

Analogously, Kuc derived a minimum-phase model for discrete-time signals for $\gamma = 1$ [35], [36], that can be easily extended to nonlinear attenuation. In this paper, we will use this formulation to describe $H_{\rm a}(f,z)$, which is detailed hereafter.

C. Causality Constraint on the Discrete-Time Impulse Response

For continuous-time signals, the causality of the system defined by the transfer function $H(f) = H_{\rm R}(f) + jH_{\rm I}(f)$ imposes that $H_{\rm I}$ is the Hilbert transform of $H_{\rm R}$ [44]. The equivalent characterization for discrete-time signals reads [45]

$$H_{\rm I}(f) = -\frac{1}{f_{\rm S}}\mathcal{P}\int_{-f_{\rm S}/2}^{f_{\rm S}/2} H_{\rm R}(g)\cot\left(\frac{\pi}{f_{\rm S}}(f-g)\right){\rm d}g, \tag{13}$$

where $f_{\rm S}$ is the sampling frequency and $\mathcal{P}$ denotes the Cauchy principal value of the integral. Taking the logarithm of $H_{\rm a}(f,z)$ in (11), $\ln H_{\rm a}(f,z) = -\alpha(f)z - j\varepsilon(f)z$, and assuming that the corresponding impulse response is causal [45] leads to

$$\varepsilon(f) = \mathcal{H}(\alpha(f)), \tag{14}$$

where $\mathcal{H}(\alpha(f))$ is defined by

$$\mathcal{H}(\alpha(f)) = -\frac{1}{f_{\rm S}}\mathcal{P}\int_{-f_{\rm S}/2}^{f_{\rm S}/2} \alpha(g)\cot\left(\frac{\pi}{f_{\rm S}}(f-g)\right){\rm d}g. \tag{15}$$

Note that this expression is well-defined for a large class of attenuation models $\alpha(f)$. Moreover, $\mathcal{H}(\alpha(f))$ has an analytic expression for linear attenuation as established in the appendix, which is useful for fast and precise computations. For power-law attenuation models with $\gamma \neq 1$, (15) can be computed by numerical integration.

The dispersion term (15) has been used in the case of linear attenuation to model attenuated signals in PMMA plates [35], [36]. Several studies precisely compared phase velocities from measured signals with the model in (14) [40], [43]. They concluded to a satisfactory agreement from materials having linear and nonlinear attenuation (PMMA, rubber, castor oil).

A synthetic example of impulse responses $h_r(t,z)$ is presented in Fig. 4. A single target is located at distance $z = 1$ mm in a homogeneous and isotropic material with propagation parameters $c_0 = 2000$ m/s, $\gamma = 1$, $\alpha_0 = 50$ Np/MHz/m, and $b(z) = 1$. Three propagation models are used: without attenuation, with linear phase (8), and with dispersive phase (14). The response without attenuation is a delta function with a shift of $t_0 = z/c_0 = 0.5$ µs. The impulse response of the linear phase model has a symmetric shape on both sides of t_0, which violates the causality condition. As expected, the impulse response of the dispersive model appears to be causal because the values are very close to zero—less than 10^{-10}—before t_0.

D. Validation With Experimental Data

We now assess the accuracy of the dispersive model and compare it with other available models. The measurements are performed using a flat circular transducer of diameter 12.7 mm and center frequency 2.25 MHz. The object under test is a 25-mm-thick PMMA plate, immersed in a water tank as illustrated in Fig. 5. The plate is in the far field of the transducer and with normal incidence. Data are acquired at sampling frequency $f_S = 100$ MHz and averaged over 100 realizations to reduce the noise level. We extract the two significant echoes from the data: the front wall echo $y_f(t)$ [Fig. 6(a)] and the back wall echo $y_b(t)$ [Fig. 6(b)]. Their respective Fourier transforms, $Y_f(f)$ and $Y_b(f)$, are plotted in moduli in Fig. 6(c), showing a strong amplitude loss and a frequency downshift between the front wall and the back wall echoes.

From (2) and (5), one has

$$Y_f(f) = b(2D)H_e(f)e^{-(\alpha_w(f)+j\beta_w(f))2D}, \tag{16}$$

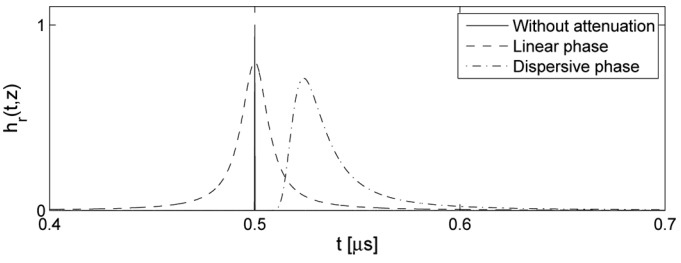

Fig. 4. Simulated impulse responses $h_r(t,z)$ using three propagation models: without attenuation, with linear phase, and with dispersive phase. Parameters: $c_0 = 2000$ m/s, $\gamma = 1$, $\alpha_0 = 50$ Np/MHz/m, $z = 1$ mm, and $b(z) = 1$. The minimum time of flight is then $t_0 = z/c_0 = 0.5$ µs. This value corresponds to: 1) the position of the delta function $\delta(t - t_0)$, 2) the center of the linear-phase impulse response, and 3) the starting time of the dispersive-phase impulse response.

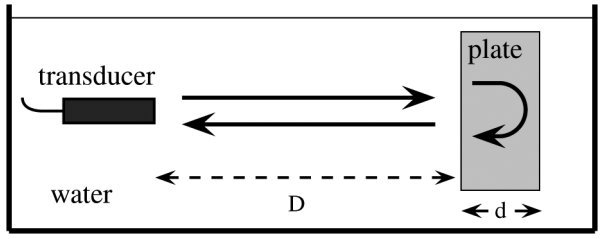

Fig. 5. Simplified data measurement setup. The plate of thickness d is placed normally in the far field of the transducer.

where $b(2D)$ is the reflection coefficient at the front face of the plate [46]. The terms $\alpha_w(f)$ and $\beta_w(f)$ stand for the propagation parameters in water [see (4)]. The back wall echo is modeled as

$$Y_b(f) = b(2D + 2d)H_e(f)e^{-(\alpha_w(f)+j\beta_w(f))2D-(\alpha(f)+j\beta(f))2d}, \tag{17}$$

with $b(2D + 2d)$ the resulting amplitude for the whole wave travel. Dividing $Y_b(f)/Y_f(f)$ enables the cancellation of $H_e(f)$ and of the terms related to the propagation in water:

$$\frac{1}{2d}\ln\left(\frac{|Y_b(f)|}{|Y_f(f)|}\right) = \alpha(f) + \frac{1}{2d}\ln\left|\frac{b(2D+2d)}{b(2D)}\right|. \tag{18}$$

Fig. 6(d) shows that such a function is approximately linear with respect to frequency, say $\alpha(f) \simeq \alpha_0|f|$. A linear regression leads to $\alpha_0 \simeq 11.55$ Np/MHz/m, which is in

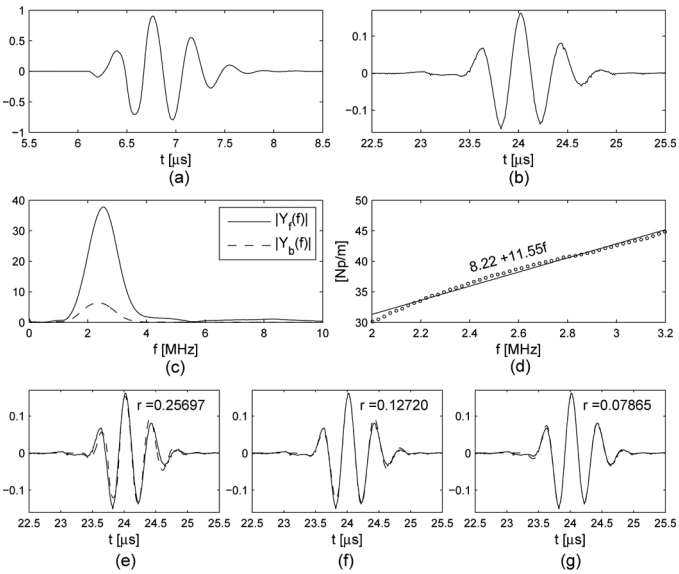

Fig. 6. Attenuation and dispersion models for data acquired from a PMMA plate with thickness $d = 25$ mm using a 2.25 MHz probe. (a) front wall and (b) back wall echoes. (c) Magnitude spectra $|Y_f(f)|$ (solid line) and $|Y_b(f)|$ (dashed line). (d) Attenuation measurement: spectral magnitude ratio $1/(2d)\ln(|Y_b(f)|/|Y_f(f)|)$ (circles) and linear regression (solid line). (e)–(g) Measured back wall echo (solid line) and three different models (dashed line), with r the quadratic error between data and model; (e) without attenuation, (f) linear phase, and (g) dispersive phase. Parameters: $c_0 = 2802$ m/s, $\alpha_0 = 11.55$ Np/MHz/m, $\gamma = 1$ (linear attenuation assumption).

agreement with the values proposed in the literature [40], [47].

By neglecting attenuation and dispersion in water, which is usually assumed in the literature [40], one has $\alpha_{\mathrm{w}}(f) = 0$ and $\beta_{\mathrm{w}} = 2\pi f/c_{\mathrm{w}}$, where c_{w} is the constant speed of sound in water. Therefore, the front wall echo is

$$Y_{\mathrm{f}}(f) = b(2D)H_{\mathrm{e}}(f)e^{-j2\pi f 2D/c_{\mathrm{w}}} \tag{19}$$

in the frequency domain, that is, in the time domain: $y_{\mathrm{f}}(t) = b(2D)h_{\mathrm{e}}(t - 2D/c_{\mathrm{w}})$. According to (17), we then fit the back wall echo $y_{\mathrm{b}}(t)$ with

$$\hat{y}_{\mathrm{b}}(t) = b(2D + 2d)h_{\mathrm{e}}(t - 2D/c_{\mathrm{w}}) * h_{\mathrm{r}}(t, 2d), \tag{20}$$

where $h_{\mathrm{e}}(t - 2D/c_{\mathrm{w}})$ is obtained from $y_{\mathrm{f}}(t)$ and $h_{\mathrm{r}}(t, 2d)$ is set from the three models introduced in Section II-B: without attenuation, with linear phase as in (8), and with dispersive phase as in (14). In the two last cases, attenuation is supposed linear, with α_0 at the previously estimated value. The velocity c_0 is calculated from $2d/(t_{\mathrm{b}} - t_{\mathrm{f}})$ where t_{f} and t_{b} stand for the front wall and back wall times of flight, respectively, yielding $c_0 \approx 2802$ m/s. For each model, the amplitudes and the times of flight of the echoes are optimized to achieve the best least-squares fit. The results are plotted in Figs. 6(e)–6(g). The quadratic error between the data $y_{\mathrm{b}}(t)$ and the model $\hat{y}_{\mathrm{b}}(t)$ is also computed and displayed on the corresponding subfigures. As expected, the dispersive model gives the best results, followed by the linear phase model.

III. A Discrete-Time Linear Model for Inverse Problems

A. Inversion Framework

Let us consider a propagation medium composed of an unknown distribution of point-like targets. From (6) and (12), the received signal is then the sum over all the target contributions:

$$\begin{aligned} y(t) &= \int_z h_{\mathrm{e}}(t) * h_{\mathrm{r}}(t, z)\mathrm{d}z \\ &= \int_z b(z)h_{\mathrm{e}}(t) * h_{\mathrm{a}}(t - z/c_0, z)\mathrm{d}z \\ &= \int_z b(z)\Big(\int_u h_e(u)h_{\mathrm{a}}(t - u - z/c_0, z)\mathrm{d}u\Big)\mathrm{d}z, \end{aligned} \tag{21}$$

where $b(z)$ describes the material spatial content independently of the ultrasonic wave propagation effects. In this context, inversion aims at reconstructing such a function from a finite number of noisy samples of $y(t)$. The reconstruction procedure might incorporate some prior knowledge on $b(z)$. For example, from an acquired A-scan in NDT, $b(z)$ may be a spike train containing the spatial positions of the acoustical impedance changes [7]:

$$b(z) = \sum_{k=1}^{K} b_k \delta(z - z_k), \tag{22}$$

where unknown parameters z_k and b_k represent the position of the kth impedance discontinuity and the associated amplitude, respectively. In the case in which no attenuation is taken into account, that is, $h_{\mathrm{a}}(t,z) = \delta(t)$, (21) and (22) formulate the classical spike train deconvolution problem that has been widely addressed in the literature [6]–[8].

Note that such a formulation can be extended to bi-dimensional data such as B-scan images. It can also be adapted to two-dimensional data in ultrasonic image restoration [4], [9] and SAFT [13]–[15].

B. A Linear Model Including Attenuation and Dispersion

Let us consider the discrete-time signal $y_n = y(n\Delta_t)$, $n = 0, \ldots, N_y - 1$, where $\Delta_t = 1/f_{\mathrm{S}}$ is the sampling period. From (21), one has

$$y_n = \int_z b(z) \int_u h_{\mathrm{e}}(u)h_{\mathrm{a}}(n\Delta_t - u - z/c_0, z)\mathrm{d}u\mathrm{d}z. \tag{23}$$

Discretizing the time integral at rate Δ_t yields:

$$\begin{aligned} y_n &\simeq \int_z b(z)\Delta_t \sum_m h_{\mathrm{e}}(m\Delta_t)h_{\mathrm{a}}\left((n - m)\Delta_t - \frac{z}{c_0}, z\right)\mathrm{d}z \\ &= \Delta_t \sum_m h_{\mathrm{e}}(m\Delta_t) \int_z b(z)h_{\mathrm{a}}\left((n - m)\Delta_t - \frac{z}{c_0}, z\right)\mathrm{d}z. \end{aligned} \tag{24}$$

Note that using the data sampling period for the discretization rate is a practical choice that is commonly made in inverse problems. In particular, it yields a Toeplitz matrix structure that can be exploited for fast computations [48]. In [49], we have recently proposed a model with higher discretization rate, showing better estimation performance in some spike train deconvolution problems—but under the usual framework $h_{\mathrm{a}}(t, z) = \delta(t)$. In this paper, we restrict the description to the discretization at rate Δ_t for the sake of clarity.

Similarly, the spatial integral is discretized at a given step size Δ_z:

$$y_n \simeq \Delta_t\Delta_z \sum_m h_{\mathrm{e}}(m\Delta_t) \sum_i b(i\Delta_z)h_{\mathrm{a}}\left((n - m)\Delta_t - \frac{i\Delta_z}{c_0}, i\Delta_z\right). \tag{25}$$

A natural choice is to consider Δ_z corresponding to the data time sampling $\Delta_z = c_0\Delta_t$. We then obtain

$$y_n \simeq \Delta_t\Delta_z \sum_m h_{\mathrm{e}}(m\Delta_t) \sum_i b(i\Delta_z)h_{\mathrm{a}}((n - m - i)\Delta_t, i\Delta_z). \tag{26}$$

Let us now denote $x_i = \Delta_t\Delta_z b(i\Delta_z)$ and let us consider the column vectors $\mathbf{y} = [y_0, \ldots, y_{N_y-1}]^{\mathrm{T}}$ and $\mathbf{x} = [x_0, \ldots, x_{N_x-1}]^{\mathrm{T}}$,

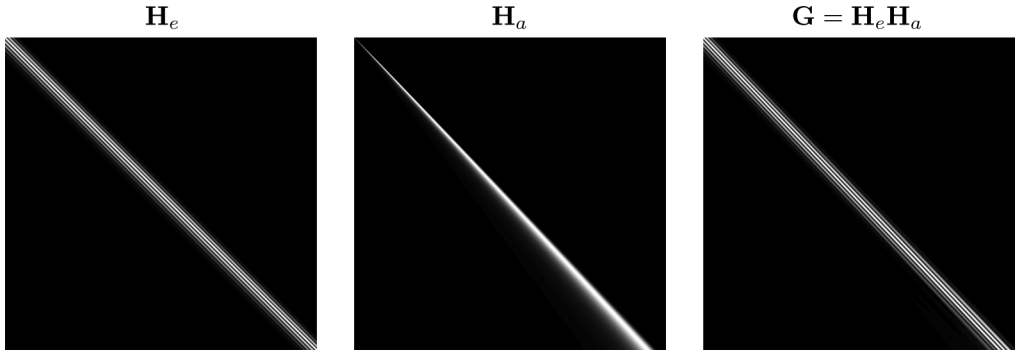

Fig. 7. Example of matrices $\mathbf{H}_\mathrm{e}$, $\mathbf{H}_\mathrm{a}$, and $\mathbf{G}$, where each column is normalized for representation clarity. $\mathbf{H}_\mathrm{e}$ is the instrumental convolution matrix obtained from the front wall echo in Fig. 6. In $\mathbf{H}_\mathrm{a}$, each line corresponds to an instant $t_n = n\Delta_t$ and each column corresponds to a spatial distance $z_i = i\Delta_z$. $\mathbf{H}_\mathrm{a}$ depends on both the attenuation and dispersion models. In this example, $\alpha(f) = \alpha_0|f|$ with $\alpha_0 = 50$ Np/MHz/m. The dispersion is set using the model in (14). The matrix $\mathbf{G}$ combines both instrumental and attenuative effects.

where the superscript T denotes matrix transposition. Note that N_x and N_y are not necessarily equal, depending on the boundary assumptions of the convolution [8]. We finally obtain the matrix-vector model:

$$\mathbf{y} = \mathbf{H}_\mathrm{e}\mathbf{H}_\mathrm{a}\mathbf{x} + \mathbf{e} = \mathbf{G}\mathbf{x} + \mathbf{e}, \tag{27}$$

where

- $\mathbf{H}_\mathrm{e}$ is the convolution matrix corresponding to the instrumental response with elements $\{h_\mathrm{e}((p-q)\Delta_t)\}_{p=0,\ldots,N_y-1, q=0,\ldots,N_x-1}$, where p and q, respectively, are the line and column indices. This matrix has a Toeplitz structure.
- $\mathbf{H}_\mathrm{a}$ is the attenuation matrix with elements $\{h_\mathrm{a}((n-i)\Delta_t, i\Delta_z)\}_{n=0,\ldots,N_x-1, i=0,\ldots,N_x-1}$. That is, the ith column of $\mathbf{H}_\mathrm{a}$ corresponds to the radiation impulse response at distance $z_i = i\Delta_z$. In our approach, it is computed from $H_\mathrm{a}(f, i\Delta_z)$ in (11), with the power-law attenuation model in (7) and the corresponding dispersive phase model defined by (14). In practice, $H_\mathrm{a}(f, i\Delta z)$ is evaluated on a frequency grid in $[-f_\mathrm{S}/2, f_\mathrm{S}/2]$ with thin spacing such that temporal aliasing can be neglected. Then, the impulse response $h_\mathrm{a}((n-i)\Delta t, i\Delta z), n = 0, \ldots, N_x - 1$ is obtained by inverse discrete Fourier transform. Causality is imposed by setting $h_\mathrm{a}((n-i)\Delta t, i\Delta z) = 0$ for $n < i$. Consequently, $\mathbf{H}_\mathrm{a}$ is lower triangular.
- $\mathbf{G} = \mathbf{H}_\mathrm{e}\mathbf{H}_\mathrm{a}$ combines the effects of the instrumental impulse responses and of the radiation impulse responses.
- $\mathbf{x}$ is the unknown sequence describing the target distribution.
- $\mathbf{e}$ is a perturbation term accounting for noise and model errors.

An example of matrices $\mathbf{H}_\mathrm{e}$, $\mathbf{H}_\mathrm{a}$, and $\mathbf{G}$ is given in Fig. 7. The matrix $\mathbf{H}_\mathrm{e}$ is built from the front wall echo in Fig. 6(a). The matrix $\mathbf{H}_\mathrm{a}$ is generated from the linear attenuation model $\alpha(f) = \alpha_0|f|$ and the dispersive relation defined in (14), with $\alpha_0 = 50$ Np/MHz/m. An example of data generated from the columns 200 and 1000 of the previous matrix $\mathbf{G}$ is also plotted in Fig. 8. Note that attenuation provokes the widening of the second echo. Dispersion causes a phase distortion that creates a time shift of the echo envelope. Indeed, in $\mathbf{H}_\mathrm{a}$, the maximum of each column is down-shifted away from the diagonal.

The model (27) states that data $\mathbf{y}$ are a noisy linear combination of columns of $\mathbf{G}$, and $\mathbf{x}$ collects the associated weights. Estimating $\mathbf{x}$ from $\mathbf{y}$ is an inverse problem that cannot be satisfactorily inverted in a least-squares sense: the matrix $\mathbf{G}$ is ill-conditioned and the generalized inverse $(\mathbf{G}^\mathrm{T}\mathbf{G})^{-1}\mathbf{G}^\mathrm{T}\mathbf{y}$ therefore suffers from uncontrolled noise amplification [8]. In the preceding example, the condition number of matrix $\mathbf{G}$ (which is a 1500×1500 matrix) is approximately $9 \cdot 10^{19}$.

C. Comparison With Olofsson's Model

From (5), the radiation transfer function at $z_i = i\Delta_z$ reads

$$\begin{aligned} H_\mathrm{r}(f, z_i) &= b(z_i)e^{-[\alpha(f)+j\beta(f)]i\Delta_z} \\ &= b(z_i)[e^{-(\alpha(f)+j\beta(f))\Delta z}]^i \\ &= b(z_i)P(f)^i. \end{aligned} \tag{28}$$

It corresponds, up to a multiplicative constant, to the ith power of the frequency kernel $P(f) = e^{-(\alpha(f)+j\beta(f))\Delta z}$. Let ρ_n, $n = 0, \ldots, N-1$ represent the discrete-time sequence with Fourier transform $P(f)$ for $f \in [-f_\mathrm{S}/2, f_\mathrm{S}/2]$. It represents the radiation impulse response

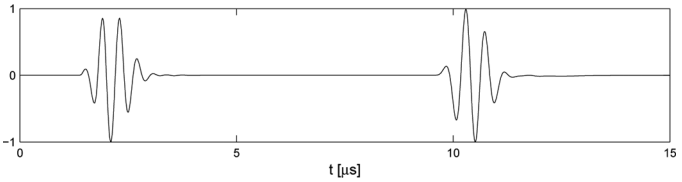

Fig. 8. Example of signal generated from the matrix $\mathbf{G}$ in Fig. 7. The data $\mathbf{y}$ are computed from the columns 200 and 1000 of matrix $\mathbf{G}$ such that: $\mathbf{y} = \mathbf{g}_{200} + \mathbf{g}_{1000}$ where $\mathbf{g}_i$ is the ith column of $\mathbf{G}$. Both echoes are normalized in amplitude for visualization clarity.

between two elementary spatial layers, separated by Δ_z. Eq. (28) states that the radiation impulse response at z_i is equal to $i-1$ self-convolutions of the time kernel ρ.

In a time-domain setting, Olofsson and Stepinski [7] proposed an empirical choice for the kernel ρ, defined by

$$\rho_0 = 0, \quad \rho_1 = 1-a, \quad \rho_2 = a, \text{ and } \rho_n = 0 \quad \forall\ n \geq 3, \tag{29}$$

with $a > 0$ and close to zero. Such a kernel implies a small distortion between two elementary layers spaced by Δ_z and is hence close to a delayed Kronecker delta function. Because of its first zero, this kernel generates causal impulse responses in $\mathbf{H}_\mathrm{a}$. The transfer function between two elementary layers consequently behaves as a low-pass filter:

$$|P(f)|^2 = 1 - 4a(1-a)\sin^2(\pi\Delta_t f). \tag{30}$$

The corresponding attenuation function can be found by

$$\alpha(f) = -\frac{\ln|P(f)|}{\Delta_z}. \tag{31}$$

Such a model has shown satisfactory results in a deconvolution context [7]. However, it seems less accurate in terms of physical reality, because $\alpha(f)$ is more adequately modeled by a frequency power law. In addition, the tuning of parameter a looks somehow arbitrary, whereas frequency-based models can be tuned according to physical models, or even set from a material catalog [47]. An example of radiation transfer functions $|H_\mathrm{r}(f,z)|$ for Olofsson's model is plotted in Fig. 3(b) for $a = 0.2$. As will be shown in Section IV-C, this value yields a model which can be compared with the linear attenuation model with $\alpha_0 = 50$ Np/MHz/m at propagation distance $z = 10$ mm. However, the two attenuation models yield quite different radiation transfer functions for other distances, as the comparison between Figs. 3(a) and 3(b) shows. The performances of frequency-based models and of Olofsson's model are compared for basic experimental data in the following section.

IV. Model Exploitation in the Case of a Single Echo: Estimation of Material Parameters

A. Single Echo Detection by Matched Filtering

We consider data made up of two well-separated echoes in a configuration similar to the one of Figs. 5 and 6. The instrumental response h_e is identified from the front wall echo, from which the matrix $\mathbf{H}_\mathrm{e}$ in (27) is built. The matrix $\mathbf{H}_\mathrm{a}$ depends on the considered attenuation model. Identifying the back wall echo then amounts to selecting the column of matrix $\mathbf{G}$, say $\mathbf{g}_i$, that best fits the data.[2]

[2]In practice, the contribution of the front wall echo is previously removed from the data.

That is, $\mathbf{x}$ should have only one nonzero coefficient at index $\hat{i}$ that corresponds to the spatial position $z_{\hat{i}} = \hat{i}\Delta_z$ of the back surface. Consider the minimization of the least-squares misfit criterion between the data and the model:

$$(\hat{i}, \hat{x}_{\hat{i}}) = \underset{i=0,\ldots,N_x-1, x_i\in\mathbb{R}}{\arg\min} \|\mathbf{y} - \mathbf{g}_i x_i\|^2, \tag{32}$$

which statistically corresponds to the maximum likelihood estimation of the one-column model $\mathbf{y} = \mathbf{g}_i x_i + \mathbf{e}$ under the assumption that the noise samples in $\mathbf{e}$ are zero-mean, independently, identically, and normally distributed [8]. Because this problem is linear in x_i, the best $\hat{x}_i$ can be found for a given $\mathbf{g}_i$ by

$$\hat{x}_i = \frac{\mathbf{g}_i^\mathrm{T}\mathbf{y}}{\|\mathbf{g}_i\|^2}. \tag{33}$$

By inserting (33) into (32), after simple manipulations, the optimal position $\hat{i}$ is

$$\hat{i} = \underset{i=0,\ldots,N_x-1}{\arg\max} \frac{|\mathbf{g}_i^\mathrm{T}\mathbf{y}|}{\|\mathbf{g}_i\|^2}. \tag{34}$$

Finally, the estimated echo is obtained by $\hat{\mathbf{y}} = \mathbf{g}_{\hat{i}}\hat{x}_{\hat{i}}$. Such a procedure follows a matched filtering approach in that it selects the column in $\mathbf{G}$ that yields the maximum correlation with data $\mathbf{y}$—up to a normalization term. However, it is not strictly speaking a matched filter; $\mathbf{G}$ is not a convolution matrix because of the spatially variant nature of the attenuation matrix $\mathbf{H}_\mathrm{a}$.

B. Joint Estimation of the Attenuation Parameter and Sound Velocity

For a frequency power-law attenuation model $\alpha(f) = \alpha_0|f|^\gamma$ with given γ, the previous echo detection procedure enables the joint estimation of the attenuation parameter α_0 and the reference velocity c_0, which are physical quantities of interest for a given material. Indeed, the attenuation transfer function in (11) at distance $z_i = i\Delta_z$ is

$$\begin{aligned} H_\mathrm{a}(f, z_i) &= e^{-[\alpha(f) + j\mathcal{H}(\alpha(f))]i\Delta_z} \\ &= e^{-[|f|^\gamma + j\mathcal{H}(|f|^\gamma)]\alpha_0 c_0 i\Delta_t}. \end{aligned} \tag{35}$$

Hence, for a given γ, the model (11) only depends on the single parameter $\chi_0 = \alpha_0 c_0$. For each χ_0, the velocity c_0 can be deduced from the optimal position $\hat{i}$, found by the matched filter as in (34), and from the thickness of the plate d by

$$c_0 = \frac{2d}{\hat{i}\Delta_t}. \tag{36}$$

The associated attenuation parameter is then given by $\alpha_0 = \chi_0/c_0$. As mentioned in Section II-B, c_0 is not the group velocity but the phase velocity for $f = \infty$. Note that

standard nondestructive evaluation (NDE) methods generally rely on the estimation of the group velocity because dispersion is not considered.

In practice, we can apply the matched filtering procedure for different values of χ_0 in an arbitrarily thin grid, and select the best value $\hat{\chi}_0$ that minimizes the residue between the data and the model $r = \|\mathbf{y} - \hat{\mathbf{y}}\|/\|\mathbf{y}\|$. This value consequently leads to $\hat{c}_0$ and $\hat{\alpha}_0$ that are the best estimations in a least-squares sense of those material quantities for a given propagation model. This procedure can be used for NDE which attempts to estimate the material properties. However, it can only be applied if the front wall and the back wall echoes are well separated.

Note that if the mechanical properties of the material are known, c_0 can be obtained from the analytic formula of the sound speed of longitudinal waves [1]:

$$c_0 = \sqrt{\frac{E(1-\nu)}{\rho(1+\nu)(1-2\nu)}}, \tag{37}$$

where E is the Young's modulus, ν is the Poisson's ratio, and ρ is the density.

C. Application to Polycarbonate

We apply this method to estimate the attenuation and velocity parameters of a homogeneous material. The same measurement configuration as in Section II-D is designed with a 2.25-MHz center frequency transducer used in pulse–echo mode. We use a clear polycarbonate plate of thickness $e = 10.2$ mm, known to have linear attenuation ($\gamma = 1$) and to be highly attenuative [5], [47]. The thickness is measured with a digital caliper, with precision ± 0.1 mm, accounting for both instrument imprecision and irregularities of the plate.

We compare the estimations obtained with the following propagation models:

1) without attenuation,
2) with linear attenuation and linear phase,
3) with linear attenuation and dispersive phase, and
4) Olofsson's model.

For Olofsson's model, we select parameter a in (29) that best fits the echo. The corresponding matched filtering procedure also yields an estimation of c_0—see (36)—but it does not provide any estimation of α_0. The residue values of the estimated back wall echoes are displayed in Figs. 9(a) and 9(b), as a function of χ_0 for linear attenuation models and of a for Olofsson's model, respectively.

One can clearly see that the dispersive model produces the lowest residue ($r \sim 0.08$). The linear phase model and Olofsson's model lead to approximately the same residue, $r \sim 0.27$ and $r \sim 0.25$, respectively. The estimated waveform without attenuation shows the greatest discrepancy with the data ($r \sim 0.45$). Because of the poor adequacy of the model, the matched filter returns a positive amplitude $\hat{x}_{\hat{i}}$ whereas a negative value is expected. Indeed the reflection coefficient between polycarbonate and water is negative [46]. As a consequence, a better estimated waveform should be left-shifted by half the wave cycle. The corresponding values of $\hat{c}_0$ and $\hat{\alpha}_0$ are listed in Table I. The attenuation parameter given by the dispersive model is 54.1 Np/MHz/m, and that obtained from the linear phase model is 52.1 Np/MHz/m. Both are in the range of the values reported in the literature (for example, 50 to 57 Np/MHz/m in [47]). We consider the value given by the dispersive model as more likely as this model yields the lowest estimation residual. The optimal attenuation parameter of Olofsson's model is 0.210, but it cannot be linked to any reference value.

As expected, the linear phase model that considers a constant phase velocity $c(f)$ leads to $\hat{c}_0 = 2274$ m/s, very close to the reference group velocity given in [47]: 2270 m/s. The value returned by the dispersive model, 2380 m/s, is logically larger than the group velocity, because it corresponds to the phase velocity at infinite frequency (see Section II-B). Olofsson's model leads to 2749 m/s, which is difficult to interpret. The inaccurate modeling obtained with the nonattenuated waveform leads to an estimated velocity of 2329 m/s, whereas it should return the same value as the linear phase model because both models consider constant phase velocity.

In this study, the dispersive model gives accurate results for polycarbonate, for which frequency-dependent attenuation can be well represented by a linear model. Such an approach could also be applied to nonlinear attenuation models with given γ, e.g., for synthetic rubber and castor oil [40].

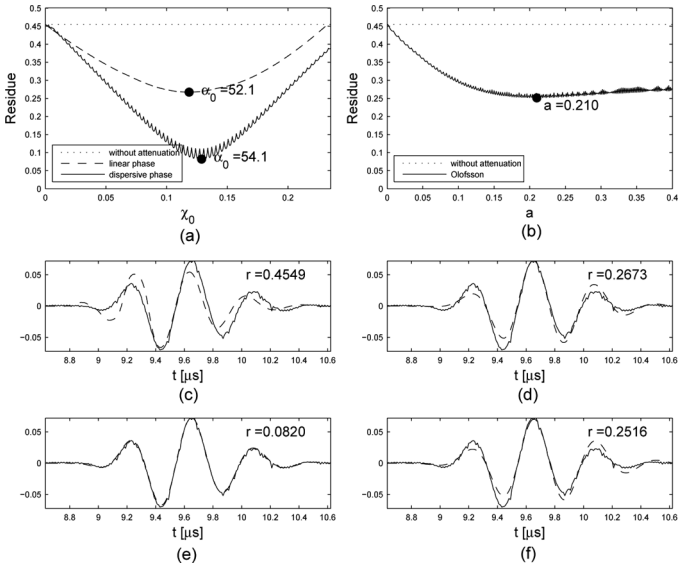

Fig. 9. Matched-filtering-based back wall echo estimation from a polycarbonate plate of thickness $d = 10.2$ mm using a 2.25-MHz transducer. (a) Residue of estimation as a function of the parameter χ_0, for several models of linear attenuation (without attenuation, linear phase, dispersive phase). (b) Residue of estimation as a function of the parameter a for Olofsson's model. (c)–(f) Data $\mathbf{y}$ (solid line) and estimation $\mathbf{y}$ (dashed line) with the optimal attenuation parameters, (c) without attenuation, (d) with linear phase, (e) with dispersive phase, and (f) with Olofsson's model (r is the residue).

TABLE I. ESTIMATED $\hat{\chi}_0$, TIMES OF FLIGHT, REFERENCE VELOCITIES, AND ATTENUATION COEFFICIENTS FOR A 10.2-MM-THICK PLATE OF POLYCARBONATE USING A 2.25-MHZ PROBE.

	$\hat{\chi}_0$	$\hat{i}\Delta_t$ (μs)	$\hat{c}_0$ (m/s)	$\hat{\alpha}_0$ (Np/MHz/m)
1 Without attenuation		8.76	2329	
2 Linear phase	0.118	8.97	2274	52.1
3 Dispersive phase	0.129	8.57	2380	54.1
4 Olofsson's model		7.42	2749	

For models 2 and 3, $\gamma = 1$.

V. APPLICATION TO THE DECONVOLUTION OF NDT DATA: ESTIMATION OF THE THICKNESS OF A PLATE

In this section, an inverse problem of spike train deconvolution is considered. From a pulse–echo measurement, our goal is to estimate the thickness of the polycarbonate plate that was already used in Section IV-C. More precisely, we consider the problem of estimating a spike train $\mathbf{x}$ from data $\mathbf{y} = \mathbf{G}\mathbf{x} + \mathbf{e}$, where the locations of the spikes—the nonzero elements in vector $\mathbf{x}$—correspond to the positions of the echoes. The distance between consecutive spikes then corresponds to twice the plate thickness.

Such a framework can be applied to a large variety of practical NDT problems [1] to measure the thickness of a layer or a wall. Applications occur for the manufacture of pipes, plates, strips, etc., and for the control of walls in severe environments (power plants, chemical industry), when the back area is out of reach. In such cases, a pulse–echo acquisition may be an appropriate solution. Note that, in the presented example, the echoes are well separated; hence the deconvolution problem is not complex from an informational point of view. In the case of thinner layers, the reflected echoes overlap and advanced processing methods such as deconvolution are appropriate tools to estimate the positions of the echoes.

Here, we use a transducer with 5 MHz center-frequency. Compared with the 2.25-MHz transducer used in the previous experiment, better resolution is expected but the attenuation effect is stronger. The back wall echo is strongly distorted and highly attenuated in amplitude, with a very low signal-to-noise ratio [see Figs. 10(a) and 10(b)]. A direct time-of-flight identification by visual inspection might lead to inaccurate thickness estimation because of the low signal-to-noise ratio and of the phase shift.

Deconvolution is performed through the minimization of the least-squares data misfit function, penalized by the ℓ_1-norm $||\mathbf{x}||_1 = \sum_i |x_i|$:

$$\mathbf{x} = \arg\min_{\mathbf{x}} \|\mathbf{y} - \mathbf{G}\mathbf{x}\|^2 + \lambda \|\mathbf{x}\|_1 . \tag{38}$$

Such a sparsity-inducing penalization produces few nonzero elements in the solution for appropriate λ. Criterion (38) is a convex function and admits a unique minimum for a given λ. The regularization parameter λ introduces a trade-off between the least-squares fit and the penalization. The value $\lambda = 0$ corresponds to the least-squares solution, which is not acceptable because of the ill-posedness of the problem [8]. Then, as λ increases, the number of spikes in $\mathbf{x}$ tends to decrease. This kind of formulation has attracted a great interest in inverse problems in the past decades [50], and particularly in ultrasonic deconvolution problems [6], [8]. Optimization is performed using the homotopy continuation method described in [51]. In this part, λ is set manually to retrieve one spike in the area of 10 mm.

We consider deconvolution using the attenuation-free model and the model with attenuation and dispersion. The first model is the approach commonly adopted in deconvolution problems. The matrix $\mathbf{G}$ is equal to $\mathbf{H}_e$, which is built from the front wall echo shown in Fig. 10(a). The second model includes $\mathbf{G} = \mathbf{H}_e\mathbf{H}_a$ where $\mathbf{H}_a$ is built from the dispersive model (11). Its parameters are set from the experimental results in Table I. We have seen in Section IV-C that the estimation of c_0 for the model without attenuation was erroneous. Hence, for this model, we set c_0 to the most plausible estimated group velocity; that is, 2274 m/s. Note that the sampling frequency is 100 MHz, leading to the spatial precision $\Delta_z = c_0\Delta_t = 0.0274$ mm and 0.0238 mm for the two models, respectively. Accord-

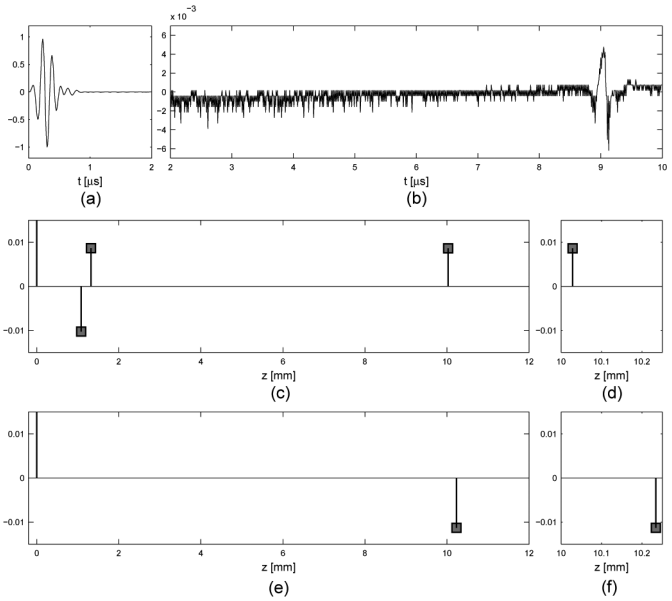

Fig. 10. Deconvolution of data acquired from a polycarbonate plate of thickness $d = 10.2$ mm with a 5-MHz transducer. (a) Data for $t \in [0, 2]$ μs corresponding to the front wall echo, (b) data for $t \in [2, 10]$ μs where a zoom in amplitude is performed. (c), (d) Deconvolution without attenuation model ($c_0 = 2274$ m/s). (e), (f) Deconvolution with linear attenuation and dispersive model ($c_0 = 2380$ m/s, $\gamma = 1$, $\alpha_0 = 54.1$ Np/MHz/m).

ing to [46], the true sequence is composed of a positive spike at 0 mm and of a negative spike at 10.2 mm.

Results are shown in Figs. 10(c)–10(f). Deconvolution with the attenuation-free model estimates four spikes. They correspond to the front wall position, two false detections and the back wall position. The last spike has a positive amplitude, which is inconsistent with the truth (as in Section IV-C). The corresponding thickness estimation is 10.5 mm. As shown in Figs. 10(e) and 10(f), the result using attenuation and dispersion in the model shows two spikes that correspond to the front wall and the back wall positions. They have a positive and a negative sign respectively, which is coherent with the expected object. The estimated distance is 10.23 mm, which is closer to the measured value. Using the model with attenuation and dispersion in criterion (38) achieves more accurate spike detection than the standard convolution model with $\mathbf{G} = \mathbf{H}_{\mathrm{e}}$, and hence leads to more satisfactory thickness estimation.

VI. Discussion and Future Works

We have presented a discrete model of ultrasonic signals that considers attenuation and dispersion. The model is built in the frequency domain, where specific radiation transfer functions are computed for a finite set of distances. We obtain a linear model between the data and the unknown spatial distribution of targets. Compared with the usual formulation, it amounts to introducing an attenuation matrix depending on acoustic propagation parameters. Experimental results from attenuative materials reveal the accuracy of such a formulation for the modeling of the backscattered echoes. Better results are obtained compared with the non-causal model that considers constant phase velocity [3] and to the causal empirical model proposed in [7]. The proposed model also yields the best results on the problem of detecting and locating the back wall echo in a polycarbonate plate. Finally, we consider a spike train deconvolution problem based on ℓ_1-norm regularization to estimate the thickness of a plate. With the proposed model, the back wall echo blurred into noise is successfully located, whereas the solution based on the standard model shows false detections and an imprecise echo location.

Future works could concern the application of the developed model to more complex data, in particular to the deconvolution of A-scans with overlapping echoes. In such cases, the better adequacy of the proposed model should improve the spike detection performance compared with standard deconvolution approaches using the generic, stationary, convolution model. We also expect that algorithms based on such a model can yield better performance than parametric models [23], [24], which also allow some flexibility in the echo shapes but do not integrate any constraint resulting from the ultrasound propagation properties.

Similar models for ultrasonic data could also be developed for two- and three-dimensional acquisitions. In particular, our approach could be extended for modeling SAFT [13], [14] and full matrix capture [15] data in ultrasonic imaging.

We have seen that our model depends on a reference velocity, which corresponds to the phase velocity at infinite frequency. The reference velocity can be obtained from the mechanical properties of the material. We have also shown that it can be estimated from a material evaluation process. In addition, complementary works could link such reference velocity to the group velocity, inspired by Gurumurthy and Arthur [32] who proposed an empirical relation between the two quantities.

Finally, our model considers a single geometrical signature of the acoustical targets, which is particularly appropriate if the targets have the same shape, as for plane surfaces in the presented experiments. Future works could include the diffraction of typical reflectors (flat-bottom holes for instance) by considering different possible signatures. In such an approach, the attenuation matrix would be replaced by a set of matrices, each one characterizing a specific diffraction signature. We believe that such dictionary-based model, coupled with efficient sparsity-aware algorithms [50], may be appropriate to address complex NDT problems for the detection and the characterization of flaws. A similar approach could be used to detect cracks or delaminations in multilayered materials. Indeed, a set of several attenuation matrices can also describe the different paths produced by multiple reflections.

Appendix
Expression of the Dispersive Phase With Linear Attenuation

With linear attenuation $\alpha(f) = \alpha_0|f|$, the phase term (15) reads $H(\alpha(f)) = -(\alpha_0 f_S)/(4\pi^2)\mathcal{J}((2\pi f)/f_S)$, with

$$\mathcal{J}(\omega) = \mathcal{P}\int_{-\pi}^{\pi} |v| \cot\left(\frac{\omega - v}{2}\right) \mathrm{d}v, \quad \omega \in [-\pi, \pi]. \tag{39}$$

Function $J(\omega)$ is odd with $J(\pi) = 0$. Consider $\omega \in \,]0, \pi[$. With $u = \omega - v$, one has

$$\mathcal{J}(\omega) = \mathcal{P}\int_{\omega-\pi}^{\omega} (\omega - u) \cot\frac{u}{2}\,\mathrm{d}u - \int_{\omega}^{\omega+\pi} (\omega - u) \cot\frac{u}{2}\,\mathrm{d}u, \tag{40}$$

where the Cauchy principal value of the first integral excludes 0 from its domain. Let $F_\omega(u)$ be an antiderivative of $(\omega - u)\cot(u/2)$. An antiderivative of $\cot(u/2)$ is $2\ln|\sin(u/2)|$. Hence, integration by parts yields for any $u \in \,]-2\pi, 2\pi[$, $u \neq 0$:

$$F_\omega(u) = 2(\omega - u)\ln\left|\sin\frac{u}{2}\right| + 2\int_0^u \ln\left|\sin\frac{\varphi}{2}\right| \mathrm{d}\varphi. \tag{41}$$

The last integral also reads

$$\int_0^u \ln\left|\sin\frac{\varphi}{2}\right| \mathrm{d}\varphi = -\mathrm{Cl}_2(u) - u\ln(2), \tag{42}$$

where $\mathrm{Cl}_2(u) = -\int_0^u \ln|2\sin(\varphi/2)|\mathrm{d}\varphi$ is the Clausen function of order 2, i.e., the imaginary part of the dilogarithm of e^{ju} [52]. From (40)–(42), one can show that

$$\begin{aligned} J(\omega) &= 2\mathrm{Cl}_2(\omega+\pi) + 2\mathrm{Cl}_2(\omega-\pi) - 4\mathrm{Cl}_2(\omega) \\ &= 4(\mathrm{Cl}_2(\omega+\pi) - \mathrm{Cl}_2(\omega)). \end{aligned} \tag{43}$$

Finally, it can be shown that (43) also holds for $w \in [-\pi, 0]$.

Acknowledgments

The authors thank A. Duclos from the University of Maine in Le Mans, France, for the help provided to perform the ultrasonic measurements and for helpful discussions about ultrasonic propagation. We also acknowledge V. Baltazart from IFSTTAR in Nantes, France, for valuable discussions about Q-filtering.

We are also grateful to the reviewers for their critical reading and valuable comments.

References

[1] J. Krautkramer and H. Krautkramer, *Ultrasonic Testing of Materials*. Berlin, Germany: Springer-Verlag, 1990.

[2] S.-K. Sin and C.-H. Chen, "A comparison of deconvolution techniques for the ultrasonic nondestructive evaluation of materials," *IEEE Trans. Image Process.*, vol. 1, pp. 3–10, Jan. 1992.

[3] A. C. Kak and K. A. Dines, "Signal processing of broadband pulsed ultrasound: Measurement of attenuation of soft biological tissues," *IEEE Trans. Biomed. Eng.*, vol. 25, pp. 321–344, Jul. 1978.

[4] M. Fatemi and A. C. Kak, "Ultrasonic B-scan imaging: Theory of image formation and a technique for restoration," *Ultrason. Imaging*, vol. 2, pp. 1–47, Jan. 1980.

[5] P. Droin, G. Berger, and P. Laugier, "Velocity dispersion of acoustic waves in cancellous bone," *IEEE Trans. Ultrason. Ferroelectr. Freq. Control*, vol. 45, pp. 581–592, May 1998.

[6] M. S. O'Brien, A. N. Sinclair, and S. M. Kramer, "Recovery of a sparse spike time series by L1 norm deconvolution," *IEEE Trans. Signal Process.*, vol. 42, pp. 3353–3365, Dec. 1994.

[7] T. Olofsson and T. Stepinski, "Minimum entropy deconvolution of pulse-echo signals acquired from attenuative layered media," *J. Acoust. Soc. Am.*, vol. 109, pp. 2831–2839, Jun. 2001.

[8] J. Idier, *Bayesian Approach to Inverse Problems*, London, UK: ISTE Ltd. and Wiley, 2008.

[9] J. A. Jensen, "Estimation of pulses in ultrasound B-scan images," *IEEE Trans. Med. Imaging*, vol. 10, pp. 164–172, Jun. 1991.

[10] J. Greenleaf, S. Johnson, S. Lee, G. Hermant, and E. Woo, "Algebraic reconstruction of spatial distributions of acoustic absorption within tissue from their two-dimensional acoustic projections," in *Acoustical Holography*, P. Green, Ed., New York, NY: Springer, 1974, pp. 591–603.

[11] G. Glover and J. C. Sharp, "Reconstruction of ultrasound propagation speed distributions in soft tissue: Time-of-flight tomography," *IEEE Trans. Sonics Ultrason.*, vol. 24, pp. 229–234, Jul. 1977.

[12] J. Greenleaf and R. Bahn, "Clinical imaging with transmissive ultrasonic computerized tomography," *IEEE Trans. Biomed. Eng.*, vol. 28, pp. 177–185, Feb. 1981.

[13] M. Karaman, L. Pai-Chi, and M. O'donnell, "Synthetic aperture imaging for small scale systems," *IEEE Trans. Ultrason. Ferroelectr. Freq. Control*, vol. 42, pp. 429–442, May 1995.

[14] F. Lingvall, T. Olofsson, and T. Stepinski, "Synthetic aperture imaging using sources with finite aperture: Deconvolution of the spatial impulse response," *J. Acoust. Soc. Am.*, vol. 114, pp. 225–234, Jul. 2003.

[15] C. Holmes, B. W. Drinkwater, and P. Wilcox, "Post-processing of the full matrix of ultrasonic transmit-receive array data for non-destructive evaluation," *NDT Int.*, vol. 38, pp. 701–711, Dec. 2005.

[16] P. A. Narayana and J. Ophir, "A closed form method for the measurement of attenuation in nonlinearly dispersive media," *Ultrason. Imaging*, vol. 5, pp. 17–21, Jan. 1983.

[17] K. Wear, "The effects of frequency-dependent attenuation and dispersion on sound speed measurements: Applications in human trabecular bone," *IEEE Trans. Ultrason. Ferroelectr. Freq. Control*, vol. 47, pp. 265–273, Jan. 2000.

[18] G. Haiat, F. Padilla, R. Cleveland, and P. Laugier, "Effects of frequency-dependent attenuation and velocity dispersion on in vitro ultrasound velocity measurements in intact human femur specimens," *IEEE Trans. Ultrason. Ferroelectr. Freq. Control*, vol. 53, pp. 39–51, Jan. 2006.

[19] D. Hale, "An inverse Q-filter," Stanford Exploration Project, vol. 26, pp. 231–244, 1981.

[20] J. M. Mendel, *Optimal Seismic Deconvolution: An Estimation Based Approach*. New York, NY: Academic, 1983.

[21] Y. Wang, *Seismic Inverse Q-filtering*. London, UK: ISTE Ltd. and Wiley, 2009.

[22] E. Kjartansson, "Constant Q-wave propagation and attenuation," *J. Geophys. Res.*, vol. 84, pp. 4737–4748, Aug. 1979.

[23] R. Demirli and J. Saniie, "Model-based estimation of ultrasonic echoes. Part I: Analysis and algorithms," *IEEE Trans. Ultrason. Ferroelectr. Freq. Control*, vol. 48, pp. 787–802, May 2001.

[24] Y. Lu and J. Michaels, "Numerical implementation of matching pursuit for the analysis of complex ultrasonic signals," *IEEE Trans. Ultrason. Ferroelectr. Freq. Control*, vol. 55, pp. 173–182, Jan. 2008.

[25] G.-M. Zhang, D. M. Harvey, and D. R. Braden, "Signal denoising and ultrasonic flaw detection via overcomplete and sparse representations," *J. Acoust. Soc. Am.*, vol. 124, pp. 2963–2972, Nov. 2008.

[26] E. Mor, A. Azoulay, and M. Aladjem, "A matching pursuit method for approximating overlapping ultrasonic echoes," *IEEE Trans. Ultrason. Ferroelectr. Freq. Control*, vol. 57, pp. 1996–2004, Sep. 2010.

[27] K. Kaaresen and E. Bolviken, "Blind deconvolution of ultrasonic traces accounting for pulse variance," *IEEE Trans. Ultrason. Ferroelectr. Freq. Control*, vol. 46, pp. 564–573, May 1999.

[28] K. Rasmussen, "Maximum likelihood estimation of the attenuated ultrasound pulse," *IEEE Trans. Signal Process.*, vol. 42, pp. 220–222, Jan. 1994.

[29] M. Fink and J.-F. Cardoso, "Diffraction effects in pulse-echo measurement," *IEEE Trans. Sonics Ultrason.*, vol. 31, pp. 313–329, Jul. 1984.

[30] P. R. Stephanishen, "Transient radiation from pistons in an infinite baffle," *J. Acoust. Soc. Am.*, vol. 49, no. 5, pp. 1629–1638, 1971.

[31] M. O'Donnell, E. T. Jaynes, and J. G. Miller, "General relationships between ultrasonic attenuation and dispersion," *J. Acoust. Soc. Am.*, vol. 63, pp. 1935–1937, Jun. 1978.

[32] K. Gurumurthy and R. Arthur, "A dispersive model for the propagation of ultrasound in soft tissue," *Ultrason. Imaging*, vol. 4, pp. 355–377, Oct. 1982.

[33] C. Lee, M. Lahham, and B. Martin, "Experimental verification of the Kramers–Kronig relationship for acoustic waves," *IEEE Trans. Ultrason. Ferroelectr. Freq. Control*, vol. 37, pp. 286–294, Jul. 1990.

[34] T. Szabo, "Causal theories and data for acoustic attenuation obeying a frequency power law," *J. Acoust. Soc. Am.*, vol. 97, pp. 14–24, Jan. 1995.

[35] R. Kuc, "Generating a minimum-phase digital filter model for the acoustic attenuation of soft tissue," in *Ultrasonics Symp.*, 1983, pp. 794–796.

[36] R. Kuc, "Modeling acoustic attenuation of soft tissue with a minimum-phase filter," *Ultrason. Imaging*, vol. 6, pp. 24–36, Jan. 1984.

[37] C.-H. Chen, W.-L. Hsu, and S.-K. Sin, "A comparison of wavelet deconvolution techniques for ultrasonic NDT," in *Int. Conf. Acoustics, Speech, and Signal Processing*, 1988, vol. 2, pp. 867–870.

[38] A. Lhémery, "Impulse-response method to predict echo-responses from targets of complex geometry. Part I: Theory," *J. Acoust. Soc. Am.*, vol. 90, pp. 2799–2807, Nov. 1991.

[39] F. A. Duck, *Physical Properties of Tissue*. London, UK: Academic Press, 1990.
[40] P. He, "Experimental verification of models for determining dispersion from attenuation," *IEEE Trans. Ultrason. Ferroelectr. Freq. Control*, vol. 46, pp. 706–714, May 1999.
[41] J. Ophir and P. Jaeger, "Spectral shifts of ultrasonic propagation through media with nonlinear dispersive attenuation," *Ultrason. Imaging*, vol. 4, pp. 282–289, Jul. 1982.
[42] J. F. Kelly, R. J. McGough, and M. M. Meerschaert, "Analytical time-domain Green's functions for power-law media," *J. Acoust. Soc. Am.*, vol. 124, pp. 2861–2872, Nov. 2008.
[43] T. Szabo, "Time domain wave equations for lossy media obeying a frequency power law," *J. Acoust. Soc. Am.*, vol. 96, pp. 491–500, Jul. 1994.
[44] A. Papoulis, *The Fourier Integral and its Applications* (McGraw-Hill electronic sciences series). New York, NY: McGraw-Hill, 1962.
[45] A. Oppenheim and R. Schafer, *Discrete-Time Signal Processing* (Prentice-Hall signal processing series). Upper Saddle River, NJ: Prentice Hall, 1989.
[46] J. Saniie and D. Nagle, "Pattern recognition in the ultrasonic imaging of reverberant multilayered structures," *IEEE Trans. Ultrason. Ferroelectr. Freq. Control*, vol. 36, pp. 80–92, Jan. 1989.
[47] A. Selfridge, "Approximate material properties in isotropic materials," *IEEE Trans. Sonics Ultrason.*, vol. 32, pp. 381–394, May 1985.
[48] G. Golub and C. Van Loan, *Matrix Computations*, vol. 3. Baltimore, MD: Johns Hopkins University Press, 1996.
[49] E. Carcreff, S. Bourguignon, J. Idier, and L. Simon, "Resolution enhancement of ultrasonic signals by up-sampled sparse deconvolution," in *Proc. IEEE Int. Conf. Acoustic, Speech and Signal Processing*, 2013, pp. 6511–6515.
[50] J. Tropp and S. Wright, "Computational methods for sparse solution of linear inverse problems," *Proc. IEEE*, vol. 98, pp. 948–958, Jun. 2010.
[51] D. M. Malioutov, M. Cetin, and A. S. Willsky, "Homotopy continuation for sparse signal representation," in *IEEE Int. Conf. Acoustics, Speech, and Signal Processing*, 2005, vol. 5, pp. 733–736.
[52] L. C. Maximon, "The dilogarithm function for complex argument," *Proc. R. Soc. Lond. A*, vol. 459, pp. 2807–2819, Nov. 2003.

Ewen Carcreff was born in Quimperlé, France, in 1984. He received the engineering degree from the ESEO school of engineering, Angers, France, in 2007 and the M.S. degree in acoustics from the University of Maine, Le Mans, France, in 2009. Mr. Carcreff worked for a few years as a Research and Development engineer in France and Japan, in the areas of audio signal processing and nondestructive testing. Since 2011, he has been pursuing a Ph.D. degree at the University of Maine in the IRCCyN laboratory, Nantes, France. His thesis interest focuses on inverse problems applied to ultrasonic nondestructive testing.

Sébastien Bourguignon was born in Dijon, France, in 1977. He received the diploma degree in electrical engineering from École Supérieure d'Électricité, Gif-sur-Yvette, France; the engineer degree from ETSIT, Universidad Politécnica de Madrid, Spain, in 2001; and the Ph.D. degree in signal processing from the University of Toulouse, France, in 2005. From 2002 to 2007, he was with the Institut de Recherche en Astrophysique et Planétologie, Toulouse, France. From 2007 to 2008, he was with IFREMER, the French research institute for exploitation of the sea, Brest, France. Then, he worked as a postdoctoral fellow at the Côte d'Azur Observatory, Nice, France. He is currently an associate professor at École Centrale de Nantes and at the Institut de Recherche en Communications et Cybernétique, Nantes, France.

His research interests include statistical inference and estimation, sparse approximation, optimization and MCMC algorithms, and applications to different kinds of observational data.

Jérome Idier is a Research Director at the Centre National de la Recherche Scientifique (CNRS). He was born in France in 1966. He received the diploma degree in electrical engineering from the Ecole Superieure d'Electricité, Gif-sur-Yvette, France, in 1988; the Ph.D. degree in physics from the Universite de Paris-Sud, Orsay, France, in 1991; and the HDR (Habilitation a diriger des recherches) from the same university in 2001. Since 1991, he has been a full-time researcher at CNRS. He was with the Laboratoire des Signaux et Systemes, Gif-sur-Yvette, France, from 1991 to 2002, and with the Institut de Recherches en Cybernetique de Nantes, France (IRCCyN) since September 2002. Since 2012, he has also been an elected member of the French National Committee of Scientific Research (CoNRS).

His major scientific interest is in statistical approaches to inverse problems for signal and image processing. More specifically, he studies probabilistic modeling, inference, and optimization issues yielded by data processing problems such as denoising, deconvolution, spectral analysis, and reconstruction from projections. The investigated applications are mainly nondestructive testing, astronomical imaging, and biomedical signal processing, and also radar imaging and geophysics. Dr. Idier has been involved in joint research programs with several specialized research centers: Electricite de France, Research and Development Division (EDF); Commissariat a l'Energie Atomique (CEA); Centre National d'Etudes Spatiales (CNES); Office National d'Etudes et de Recherches Aerospatiales (ONERA); Loreal; Thales; and Schlumberger.

Dr. Idier is the coauthor of two international patents. He has edited two books on inverse problems in the field of signal and image processing (published by Hermes Science, ISTE Ltd. and John Wiley & Sons Inc.) and he has authored 35 peer-reviewed papers and more than 110 conference papers.

He has served as an Associate Editor for the *IEEE Transactions on Signal Processing* (2010–2012) and for the *Journal of Electronic Imaging*, co-published by SPIE and IS&T, since 2009.

Laurent Simon was born in France in 1965. He received the Ph.D. degree in acoustics from the Université du Maine, Le Mans, in 1994. He is currently a professor with the Laboratoire d'Acoustique de l'Université du Maine, UMR-CNRS 6613, Le Mans. His research interests mainly concern signal processing for vibration and acoustics, including nonlinear system identification, inverse problems for NDT, and spectral estimation of missing data.